Hindawi Publishing Corporation
Journal of Spectroscopy
Volume 2015, Article ID 489162, 9 pages
http://dx.doi.org/10.1155/2015/489162

Research Article

Infrared Spectroscopic Characterization of Photoluminescent Polymer Nanocomposites

Kyle Gipson,[1] Kathryn Stevens,[2] Phil Brown,[2] and John Ballato[2]

[1] *Department of Engineering and the Center for Materials Science, James Madison University, Harrisonburg, VA 22807, USA*
[2] *Center for Optical Materials Science and Engineering Technologies (COMSET) and the Department of Materials Science and Engineering, Clemson University, Clemson, SC 29634, USA*

Correspondence should be addressed to Kyle Gipson; gipsonkg@jmu.edu

Received 22 August 2014; Accepted 20 October 2014

Academic Editor: Qingrui Zhang

Organicallycoated inorganic nanoparticles were synthesized to produce photoluminescent nanocomposites based on a polymethyl methacrylate (PMMA) matrix. The nanoparticles comprised organic ligands (acetylsalicylic acid, ASA, and 2-picolinic acid, PA) attached to the lanthanum trifluoride (LaF_3) host crystals that were doped with optically active terbium III (Tb^{3+}) and synthesized using solution-based methods. The ligands were employed to functionalize the surface of Tb^{3+}:LaF_3 nanocrystals to aid in dispersing the nanoparticles. In order to confirm the presence of the constituents within the inorganic-organic system, the nanoparticles were characterized by infrared spectroscopy and energy-dispersive X-ray spectroscopy. Absorption peaks observed from infrared spectroscopy for all the polymer nanocomposites loaded with organic surface treated nanocrystals exhibited peaks that were not present in undoped PMMA but were characteristic of the dopant and the ligand.

1. Introduction

Polymer optical materials (POMs) in devices (e.g., splitters, couplers, multiplexers, demultiplexers, and amplifiers) have been used in integrated lightwave circuits wherein polymer optical fibers and planar waveguides are combined for specific functionalities [1]. POM applications range from planar integrated optics (optical circuits on planar substrates) [2] to local area networks (LANs) [3] and sensing components for devices used for medical [4], manufacturing [5], and security applications [6]. Light-emitting polymer nanocomposites (a subset of POMs) are generally utilized in planar lightwave circuits and in telecommunication applications [1] as well as incoherent light-emitting devices, optical sensors, and photodetectors [7].

In order to create light-emitting polymer nanocomposites, various additives have been employed to change the optical properties of polymers, in particular polymethyl methacrylate (PMMA). PMMA has been shown to be a suitable matrix for optically active additives (dopants) [8]. Luminescent species that have the capability of fluorescing and being dopants to overcome attenuation are organic dyes, quantum dots, and rare-earth (RE) ions doped in inorganic nanocrystals [9–12]. In this research, the dopants studied were RE ions doped into inorganic nanocrystals. The dopant is excited upon interaction with light to a higher electronic energy level. As a result, the dopant produces radiative (photon) and nonradiative emissions (phonon) upon relaxation to a lower lying state or the ground state.

Nanoscale inorganic materials (e.g., lanthanum trifluoride, LaF_3) doped with RE (e.g., terbium, Tb^{3+}) ions typically are incompatible with organic polymers. Inorganic material dispersed in organic polymers generally favors agglomeration. Nanoscale materials tend to form agglomerates as an attempt to reduce the surface area to minimize interfacial energy [13]. Therefore, surface treating of the inorganic material with an organic species, that is, ligands, is an option for aiding inorganic-organic compatibility.

Ligands are organic molecules that have the ability to create ion complexes or attach to the surface of nanocrystals in order to aid in dispersion within the polymer matrix. Aromatic acids, bipyridines, or donor groups containing

negatively charged atoms (e.g., carboxylate or phosphate groups) are examples of ligands utilized to attach to the surface of nanocrystals via ionic attraction [14, 15]. Such organic conjugated ligands typically absorb energy in the near ultraviolet (UV) spectral region ranging from 200 nm to about 400 nm [16]. The surface treatment or "capping" of nanocrystals [1, 14] with aromatic acids [17] (acetylsalicylic acid, ASA) [18] and bipyridines (2-picolinic acid, PA) have indicated that the ligands also serve the purpose of UV light harvesting ligands that enhance fluorescence of RE emissions by absorbing and transferring energy to the dopant RE ions [19–21]. The polymer optical nanocomposite studied in this work consists of ligand capped RE-doped nanocrystals.

Infrared spectroscopy, which is considered a useful tool for classification and identification, was used to investigate the relatively small changes in the chemical structures of various molecules [22]. The focus of this research is the IR characterization of ASA and PA plus the determination of the inorganic material within the polymer nanocomposite.

2. Materials and Methods

2.1. Materials. Solvents used were anhydrous tetrahydrofuran, THF (99%—Acros), methanol (99.8%—BDH), and ultrapure water (18.2 MΩ·cm). The following items were used as received: polymethyl methacrylate, PMMA, at an approximate weight average molecular weight of 130 k from Plaskolite West, Inc., lanthanum (III) nitrate hexahydrate ($La(NO_3)_3{\cdot}6H_2O$, 99.99%—Sigma-Aldrich), terbium (III) nitrate hydrate ($Tb(NO_3)_3{\cdot}6H_2O$, 99.9%—Sigma-Aldrich), acetylsalicylic acid, ASA (MP Biomedicals, LLC), 2-picolinic acid, PA (99%—Alfa Aesar), ammonium fluoride, NH_4F (99.3%—Fisher Scientific), ammonium hydroxide, NH_4OH (28–30% ACS—BDH Aristar-VWR), ethanol, EtOH (99.5%—Acros), and acetone (99.9%—BDH).

2.2. Nanoparticle Synthesis. Tb^{3+}:LaF_3 nanocrystals were prepared in solutions with either water or methanol as the solvent and the nanoparticle syntheses are as described previously [18]. The rare-earth solution of $La(NO_3)_3{\cdot}6H_2O$ (9 mmol) and $Tb(NO_3)_3{\cdot}6H_2O$ (2 mmol) in 16 mL of solvent was prepared at room temperature. NH_4OH was added to the rare-earth solution to adjust the pH to a value of 8 for the aqueous synthesis. The pH of the methanol solution was not adjusted.

2.3. Synthetic Route 1—Water Solvent Synthesis. The rare-earth solution was added drop-wise into a stirring solution of NH_4F (11 mmol) and 20 mmol of the ligand (ASA or PA) in water at 70°C. The volume ratio of water/ligand was 40 : 1. NH_4OH was added to readjust the suspension to a pH value of 8; it was then stirred for 2 hours at 70°C. A centrifuge was used to separate the precipitate at 3000 rpm for 10 minutes. The nanoparticles (precipitate) were washed with 50 vol% of ethanol (EtOH) in water followed by an acetone wash and then dried over night in a vacuum oven at 30°C. The particles were then added to 5 wt% of PMMA in tetrahydrofuran, THF (PMMA/THF), to form a polymer nanoparticle suspension of ligand: Tb^{3+}:LaF_3:PMMA/THF, that was added drop-wise to excess (v/v of suspension to MeOH; 1 : 400) stirred in methanol (MeOH) at ~3°C. The precipitated nanocomposite polymer powder was vacuum-filtered, washed in MeOH, and then dried over night in a vacuum oven.

2.4. Synthetic Route 2—Methanol Solvent Synthesis. The rare-earth solution (prepared in manner stated in Section 2.2) was added drop-wise to a stirring solution of NH_4F (12 mmol) and 23 mmol of the desired ligand (ASA or PA) in methanol at room temperature ~25°C and was stirred for 1 hour. The volume ratio of methanol/ligand was 40 : 1. pH was monitored and in the case where ≤5% water was present in the suspension; the relative pH is stated for the solution values. A centrifuge was used to separate the precipitate at a setting of 3000 rpm for 10 minutes. The particles were washed twice with methanol. Neat MeOH (v/v of PMMA/THF to MeOH; 1 : 400) was added to resuspend the particles and the temperature of the nanoparticle suspension in excess MeOH was decreased to approximately 3°C. After 30 minutes, a solution of 5 wt% of PMMA/THF was added drop-wise to the ligand: Tb^{3+}:LaF_3:MeOH suspension. The product was precipitate nanocomposite polymer powder. The precipitate nanocomposite polymer powder was vacuum-filtered, washed in MeOH, and then dried under vacuum over night.

2.5. Attenuated Total Reflection (ATR) Infrared Spectroscopy. Samples of the ligands as well as dried nanoparticles, precipitated polymer, and precipitated polymer nanocomposite were analyzed by ATR. A Thermo-Fisher Nicolet Magna 550 FTIR spectrometer equipped with a Thermo-SpectraTech Foundation Series Diamond ATR accessory, Nic-Plan microscope, and Omnic software acquired the spectra. Sixteen scans were conducted at room temperature and the spectral resolution was set at 8 cm^{-1}.

2.6. Energy-Dispersive X-ray Spectroscopy. The compositions of the nanoparticles were characterized utilizing a scanning transmission electron microscope (STEM, Hitachi HD2000, Pleasanton, CA) equipped with an Oxford INCA Energy 200 Energy Dispersive Spectrometer (EDX). Samples were prepared by drop casting nanoparticle suspensions followed by subsequent solvent evaporation onto 200 mesh carbon coated copper TEM grids.

3. Results and Discussion

Inorganic nanoparticles doped with optically active rare-earth ions were synthesized in the presence of organic aromatic ligands. Two nanocomposite synthetic routes were evaluated as outlined in Sections 2.3 and 2.4 where the first synthesis method (Route 1) utilized water as the solvent and the second synthesis method (Route 2) utilized methanol as the solvent. After synthesis via Route 1, the nanoparticles were dried, ball milled, and dispersed in polymer/solvent solutions, which were subsequently phase inverted in methanol to form polymer nanocomposites. The work of Widiyandari et al. supported the potential use of mechanical milling

as a way to reduce agglomerates formed in nanoparticle suspensions of electrohydrodynamic atomization [23]. In this research, the dried particles and dried polymer nanocomposites were ball milled with Telfon spheres in a container that was vortex stirred.

In Route 2, nanoparticles were synthesized in methanol and were not dried. The resulting polymer/solvent solutions were phase inverted into nanoparticle suspensions in methanol to form polymer nanocomposites. Route 2 was devised to simplify the synthesis technique.

Two different aromatic ligands (acetylsalicylic acid, ASA, and 2-picolinic acid, PA) were utilized to functionalize the surface of Tb^{3+}:LaF_3 nanocrystals (NC). The ligand to nanocrystal (L : NC) molar ratio was varied for each ligand system for two reasons. Firstly, the emission intensities of terbium have been observed to be dependent on the ratio of ligand to inorganic component [24]. Secondly, the amount of ligand attached to the surface of the nanocrystal may affect nanoparticle agglomeration [25–27]. The selected aromatic ligand systems were characterized using infrared spectroscopy and optical spectroscopy.

3.1. Organic Ligand IR Characterization. Powder samples of the ligands, nanoparticles, and polymer nanocomposites were used to conduct qualitative characterizations of ATR absorption peaks. The qualitative characterizations were based on data found in literature provided by the following researchers: Binev et al. [28] and Boczar et al. [29] investigated the infrared spectra of acetylsalicylic acid, both Silverstein et al. [30] and Dean [31] work offered spectrometric identification of organic compounds, Soman and Kelkar [32] research studied infrared spectra of doped PMMA, and Świderski et al. [33] and Koczoń et al. [34] research investigated the infrared spectra of picolinic acid. The vibration modes are classified using the following symbols: ν—stretching, δ—deformation, and τ—torsion/wagging. Wavenumbers and IR band assignments for the spectra of PA (Figure 1) and ASA (Figure 2) are found in Tables 1 and 2, respectively.

Listed in Table 1 are absorption bands associated with picolinic acid and the IR spectrum is illustrated in Figure 1. The sharp peak located at 3112 cm^{-1} denotes the C–H stretching mode from the aromatic ring. The broad peak with mid-center location of 2591 cm^{-1} was attributed to the O–H stretching from the carboxylic acid. The peak located at 1706 cm^{-1} is attributed to the C=O stretching of carboxylic acid. C–H stretching from the aromatic ring is assigned to the 1658 cm^{-1} peak. Six bands represent the C–C stretching of the conjugated ring system of pyridine. Świderski et al. conducted experimental FT-IR, FT-Raman, and ^{1}H NMR and theoretical studies of metals chelated by picolinic acid where the six bands were observed at 1606, 1593, 1572, 1527, 1438, and 1339 cm^{-1} without a contribution from the C–N [33]. The bands that are at 1293 and 1083 cm^{-1} correspond to in plane deformation of C–H bonds in the pyridine ring. The absorption peak observed at 750 cm^{-1} indicates deformation of the carbons within the ring.

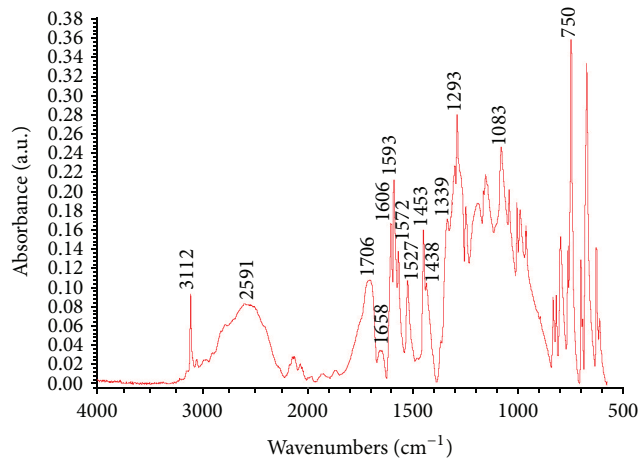

Figure 1: Infrared spectrum (4000–500 cm^{-1}) of picolinic acid.

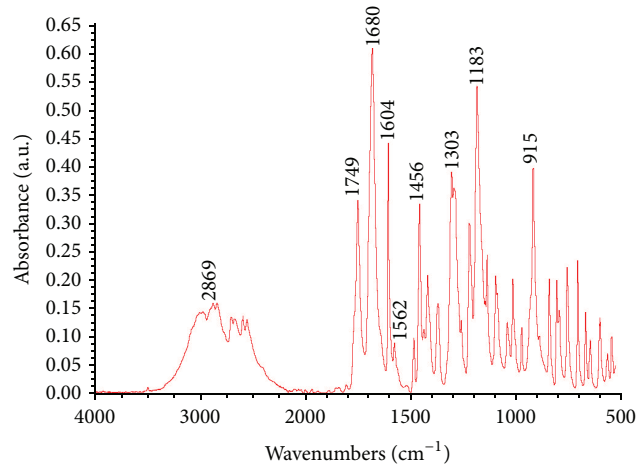

Figure 2: Infrared spectrum (4000–500 cm^{-1}) of acetylsalicylic acid.

The broad absorption peak of ASA that spans from approximately 3250 to 2500 cm^{-1} (Figure 2) contains stretching modes of the O–H group from the acid, CH_3 group attached to the ketone, and C–H bonds located on the benzene ring. C=O stretching was assigned to the peaks observed at 1749 cm^{-1} for the ester and 1680 cm^{-1} for the carboxy group. The strong peak at 1604 cm^{-1} is attributed to C–C stretching in the benzene ring, ring deformation, and C–C–C deformation [28]. The peaks located at 1562 cm^{-1} and 1456 cm^{-1} are also associated with benzene ring stretching of C=C and C–C bonds, respectively. The band at 1303 cm^{-1} is related to O–H deformation and C–C stretching of the ring. The peak observed at 915 cm^{-1} contains C–C, O–C, C–O, and C–CH_3 deformations. Deformation of the CH_3 and stretching of C–O–C and C–C bonds were assigned to the peak observed at 1183 cm^{-1}.

3.2. Nanoparticle IR Characterization. The nanoparticle constitutes the doped nanocrystal, NC (NC = Tb^{3+}:LaF_3), with attached ligand (PA or ASA). PA:NC refers to PA ligand

Table 1: Observed vibrational modes for picolinic acid [28–34].

Wavenumber (cm^{-1})	Modes of vibration	
3112	νCH (ring)	
3054	νCH (ring)	
2591	νOH (CO_2H)	
1706	νC=O (CO_2H)	
1658	νCH (ring)	
1606	νCC (ring)	
1593	νCC (ring)	
1572	νCC (ring)	
1527	νCC (ring)	
1453	νCH (ring)	νCOO
1438	νCC (ring)	
1339	νCC (ring)	
1293	δCH	
1250	δCH	
1157	δCH	
1083	δCH	
1045	δCH	
1008	νCH (ring)	
995	δCH	
965	δCH	
836	δCH	
821	δCH	
800	δCH	
764	δCH	
750	δCCC (ring)	
703	δCCC (ring)	

Table 2: Observed vibrational modes for acetylsalicylic acid [28–34].

Wavenumber (cm^{-1})	Modes of vibration		
3000–2500	νOH		
3000–3100	νCH (ring)		
2975–2950	νCH_3		
1749	νC=O (ester)		
1680	νC=O (carboxy)	νC=C	
1604	νC=O (ring)	δOH	
1562	νCC (ring)		
1456	νC=C	δCH (ring)	δCH_3
1418	δOH	δCH_3	δCOH
1368	δCH_3	νCC (ring)	δCH (ring)
1303	δCOH		
1292	δCOH		
1256	δCH (ring)		
1218	ν-O–CO–CH_3	δCH (ring)	
1183	ν-O–CO–CH_3	δCH (ring)	
1134	δCH (ring)		
1093	δCH (ring)	νCC (ring)	
1012	δ-O–CO–CH_3	δCH_3	
915	δ-O–CO–CH_3	νCC (ring)	
839	δCH (ring)		
803	δ-O–CO–CH_3	δCC (ring)	δCH (ring)
791	δCH (ring)	νCOOH	
753	δCH (ring)		
704	δCH (ring)	δCC (ring)	
666	δCH (ring)	δCOOH	δO–C=O

capped nanocrystals and ASA:NC corresponds with ASA ligand capped nanocrystals. Provided in Figures 3 and 4 are the IR spectra of PA:NC via synthesis Routes 1 and 2, respectively. Changes to the wavenumber of the observed peaks in the spectra of the nanoparticles could indicate perturbations to the ligand systems [33]. These perturbations (deformations of the uniform distribution of π-electron density within the ring) of aromatic systems may result in band elimination, band shifting to lower wavenumbers as a result of bond weakening, or band intensity reduction [33].

A representative IR spectrum for PA:NC via synthetic Route 1 is displayed in Figure 3 and via Route 2 in Figure 4. The spectra are similar and will be discussed as such. The broad peak with the mid-center point located at 3395 cm^{-1} corresponds to O–H stretching of the residual solvent.

The observed 1706 cm^{-1} peak of PA found in Figure 1 corresponds to the stretching of C=O bonds from the carboxylic acid. This peak was not observed in the study of metal picolinates (picolinic acid coordination of magnesium, calcium, strontium, and barium) [33]. However, Koczoń et al. observed the peak in picolinic acid. This work focused on experimental and theoretical IR and Raman spectra analyses of picolinic, nicotinic, and isonicotinic acids and their complexes with different metals [34]. This research indicated that stretching of the C=O from the carboxylic

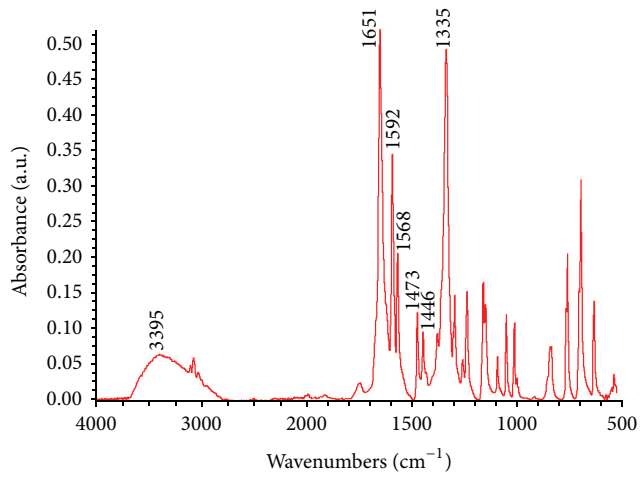

Figure 3: Infrared spectrum (4000–500 cm^{-1}) of PA:NC via synthetic Route 1 (water synthesis).

acid occurred at 1717 cm^{-1}. However they did not observe the 1706 cm^{-1} band in the spectra of the PA:NC shown in Figures 3 and 4. The absence of this peak may indicate ligand attachment to the nanocrystal.

A peak at 1651 cm^{-1} was observed in the spectra of PA:NC via Routes 1 and 2 in Figures 3 and 4, respectively.

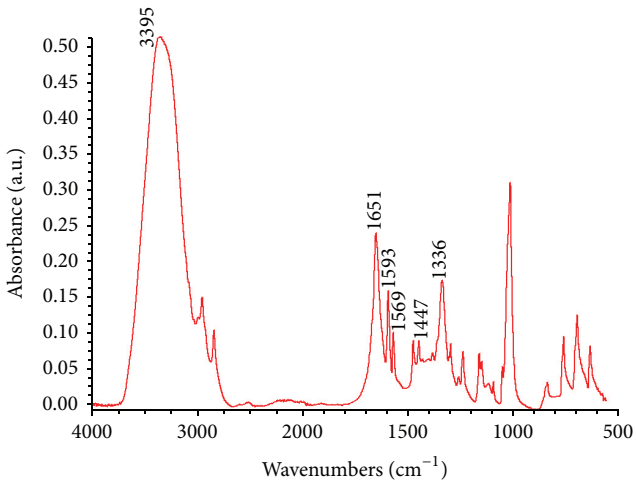

Figure 4: Infrared spectrum (4000–500 cm^{-1}) of PA:NC via synthetic Route 2 (methanol synthesis).

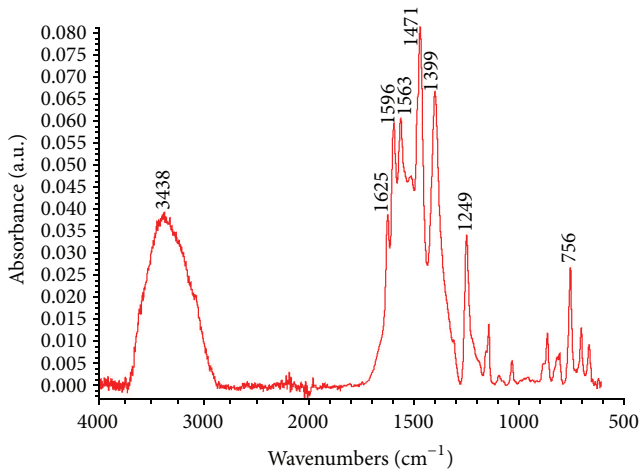

Figure 5: Infrared spectrum (4000–500 cm^{-1}) of ASA:NC via synthetic Route 1 (water synthesis).

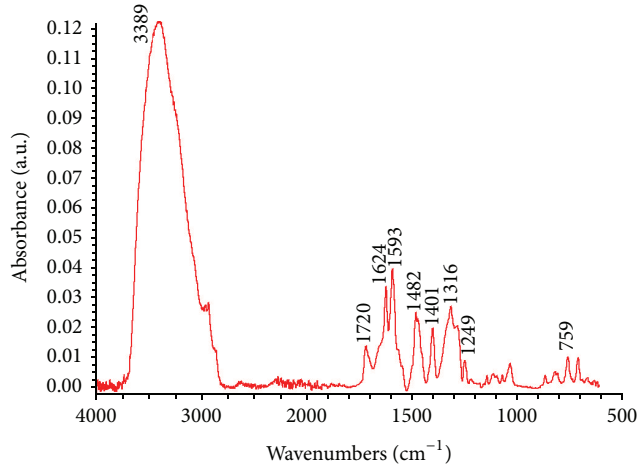

Figure 6: Infrared spectrum (4000–500 cm^{-1}) of ASA system via Route 2 (methanol synthesis).

The 1651 cm^{-1} reflects the C–O stretching of the formed anion which is not related to the peak of 1658 cm^{-1} associated with C–H stretching from the aromatic ring list in Table 1. The anion of the acid is formed as the result of ionization of the hydroxyl group.

The 1606, 1527, and 1339 cm^{-1} observed peaks of picolinic acid in Figure 1 are similar to the picolinic acid peaks at 1607, 1528, and 1343 cm^{-1} viewed by Świderski et al. These peaks are associated with stretching of the C–C bonds from the aromatic ring and were not observed in the metal picolinate spectra [33]. The lack of the 1606, 1527, and 1339 cm^{-1} peaks in this research as depicted in Figures 3 and 4 is an indication that the addition of the nanocrystals has an influence on the ligand structure.

The peaks associated with C–C stretching from the aromatic ring that are present in picolinic acid and remain in nanoparticles via Routes 1 and 2 are located at 1593 and 1572 cm^{-1} (Figure 1) for the acid and ~1593 and ~1568 cm^{-1} for the PA:NCs (Figures 3 and 4). There exists relatively little change to the peak values, which may indicate stronger vibrations as the result of perturbations in other areas of the ligand.

The IR spectra obtained for ASA:NC produced by water synthesis are shown in Figure 5 and via methanol synthesis are illustrated in Figure 6. The broad peaks located at 3438 cm^{-1} for ASA:NC via Route 1 and 3389 cm^{-1} via Route 2 are indicative of O–H stretching from the residual solvent. The 1720 cm^{-1} peak is associated with C=O stretching of the carboxy group which is observed in ASA:NC via Route 2 but not in the IR spectra for Route 1. The peaks 1625 cm^{-1} (synthetic Route 1 in Figure 5) and 1624 cm^{-1} (synthetic Route 2 in Figure 6) which were not observed in the IR spectra for ASA were indications of C=C bond stretching of the ring. Observed peaks at 1596 cm^{-1} for Route 1 and 1593 cm^{-1} for Route 2 correlate to C=O stretching with the corresponding peak in acid at 1604 cm^{-1}. O–H deformation was assigned to the peaks located at 1399 cm^{-1} for water synthesis and 1401 cm^{-1} for the methanol synthesis and both peaks were lower than the 1418 cm^{-1} peak of the acid. C–H deformation at the ring linked to the peak located at 1256 cm^{-1} of the acid was observed to occur at lower wavenumbers for the nanoparticles, 1249 cm^{-1} for both synthesis procedures. These perturbations of ligand clearly indicate an influence of the nanocrystals on the ligand.

3.3. PMMA IR Characterization. The observed vibrational modes associated with PMMA are listed in Table 3 and the IR spectrum is illustrated in Figure 7. Shown in Figure 7 is a cluster of peaks found at 2994 and 2950 cm^{-1} within the undoped precipitated PMMA spectra which typically represent CH_3, CH_2, and CH stretching. The stretching of the saturated aldehyde is generally characterized with a strong peak located around 1725 cm^{-1}. The two peaks located at ~1480 cm^{-1} and 1380 cm^{-1} may illustrate the two bands that designate C–CH_3 deformation. The CH_3 stretching may result in a peak

Table 3: Observed vibrational modes for PMMA.

Wavenumber (cm^{-1})	Modes of vibration	
2994	νCH_3	
2950	νCH_3	
1725	νCOH	
1481	$\delta C–CH_3$	
1435	νCH_3	δCOH
1387	$\delta C–CH_3$	
1266	νOC	
1239	νOC	
1190	$\nu C–C–O$	
1145	νCO	
988	τCH	
841	τCH	
750	τCH_2	$\nu C–C–O$

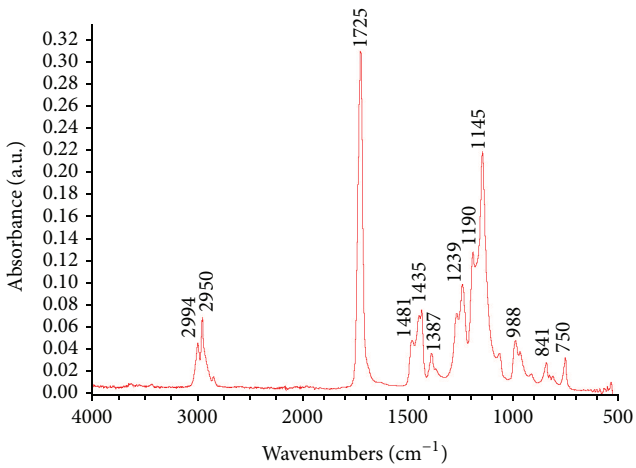

Figure 7: Infrared spectrum (4000–500 cm^{-1}) of undoped precipitated PMMA.

located approximately at 1435 cm^{-1} whereas the peaks located between 1210 and 1320 cm^{-1} and at 1145 cm^{-1} may indicate O–C and C–O stretching, respectively. The peaks located between 750 and 988 cm^{-1} may correspond to torsional deformation of CH bonds.

3.4. Polymer Nanocomposite IR Characterization. The FT-IR spectra shown in Figure 8 compare undoped precipitated PMMA (red) with ASA ligand capped nanocrystals and PA ligand capped nanocrystals dispersed in PMMA. The ASA system was synthesized to 2 : 1, 3 : 1, 4 : 1, and 5 : 1 molar ligand to nanocrystal ratio via synthetic Routes 1 and 2. PA system was also synthesized to 2 : 1, 3 : 1, 4 : 1, and 5 : 1 L:NC through water synthesis and methanol synthesis.

The green spectra represent PMMA nanocomposites composed of the PA system (PMMA:PA system) via water synthesis (dark green) and methanol synthesis (light green). The blue spectra correspond to the PMMA nanocomposites made from the ASA system (PMMA:ASA system) where the nanoparticles were synthesized in water (dark blue) and in methanol (light blue).

All the anticipated peaks for the undoped PMMA were present in the spectra of the nanoparticle loaded PMMA (PMMA nanocomposite). The IR spectra of PMMA overlapped many of the absorption bands of the ligand systems except in area of 1700–1500 cm^{-1}, inset of Figure 8 The peaks located in this area were found to correlate to peaks observed in the IR spectra of the ligands and nanoparticles.

The spectra in Figure 8 for the PMMA nanocomposite composed of the PA system (PMMA:PA:NC) via water (dark green) and methanol (light green) nanoparticle synthesis exhibited absorption peaks at 1653 cm^{-1}, 1593 cm^{-1}, and 1568 cm^{-1} that are not present in undoped PMMA. The 1653 cm^{-1} reflects the C–O stretching of the formed anion. The 1593 and 1568 cm^{-1} peaks are associated with C–C stretching in the pyridine ring. Świderski et al. observed a peak located at 1606 cm^{-1} in picolinic acid that did not appear for any of the studied metal complexes which is similar to this work where the this peak did not appear in the IR spectra of the ligand capped nanocrystals.

The C–C stretching associated with the 1568 cm^{-1} band was observed at lower wavenumber compared to the observed band (1572 cm^{-1}) in picolinic acid. The wavenumber shift was comparable with the ligand coordination of weak cations in a study conducted by Świderski et al. [33]. The wavenumber reduction may be an indication of nanocrystal influence on the perturbation on the ligand system. There was no observed change in the 1593 cm^{-1} peak.

The synthetic Route 2 of the PMMA:PA:NC produced broad peaks observed at center mid-points of 3394 cm^{-1} and 1616 cm^{-1}. The band with the center point of 3394 cm^{-1} is related to the O–H stretching associated with methanol.

The synthetic Route 2 of the PMMA:ASA:NC produced broad peaks at center mid-points of 3549 cm^{-1} representing O–H stretching that corresponds to residual solvent.

Two peaks at 1601 cm^{-1} and 1559 cm^{-1} were observed for the PMMA:ASA:NC that were not present in undoped PMMA. These bands suggest C–C stretching within the aromatic ring. The peaks were located at lower wavenumbers compared to the corresponding bands of 1604 cm^{-1} and 1562 cm^{-1} observed in ASA. In ASA:NC these peaks were located at ~1596 cm^{-1} with a shoulder at 1562 cm^{-1}. Again, these changes in vibrational signatures are an indication of nanocrystal and ligand interaction.

The work presented by Wang et al. on a one-step synthesis of $LaF_3:Yb^{3+}$ and $LaF_3:Er^{3+}$ nanocrystals in methanol without ligands reported a broad absorption band around 3412 cm^{-1} which was attributed to O–H stretching vibrations, that is, hydrogen bonding of alcohols [35, 36]. The absorption peak at 3200–3400 cm^{-1} observed in Figure 4 is similar to the work of Wang et al. These peaks do not occur in synthetic Route 1 as a result of two drying steps which eliminate the water and hence the associated OH groups. The nanoparticles are dried before incorporation into the polymer/solvent solution and the nanocomposite is dried after phase inversion.

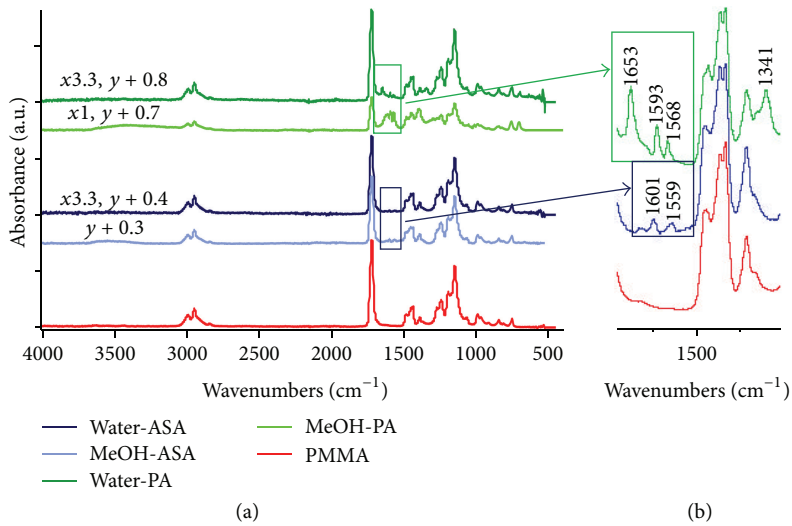

Figure 8: ATR infrared spectra (a) at 4000–500 cm^{-1} of undoped precipitated PMMA (red), ASA systems via water (dark blue) and via methanol (light blue), and PA systems via water (dark green) and via methanol (light green). (b) Inset: representation of peaks located at 1700–1500 cm^{-1}.

Table 4: Inorganic elemental composition and corresponding atomic percentage of nanoparticles synthesized in water and methanol at different molar ligand to nanocrystal ratios.

Synthetic route (solvent)	Molar ligand to nanocrystal ratio	PA : NC			ASA : NC		
		Elemental composition			Elemental composition		
		F atomic %	La atomic %	Tb atomic %	F atomic %	La atomic %	Tb atomic %
1 (water)	2 : 1	59	36	5	48	43	9
	3 : 1	46	46	8	61	31	8
	4 : 1	43	49	8	60	32	8
	5 : 1	64	31	5	62	31	7
2 (MeOH)	2 : 1	65	26	9	66	24	10
	3 : 1	54	36	10	67	24	9
	4 : 1	62	28	10	70	23	7
	5 : 1	64	22	14	61	31	8

3.5. Elemental Analysis of Inorganic Component of Ligand Capped Nanocrystal. The results of the elemental composition of the nanoparticles determined by energy dispersive X-ray (EDX) spectroscopy are summarized in Table 4. The ligand to nanocrystal ratios were calculated based on the molar concentrations of the ligand to those of the sum of La^{3+} and Tb^{3+}. The calculated atomic percentages were as follows: F, 75%, La, 20%, and Tb, 5%.

Data analysis through EDX confirmed the existence of Tb, La, and F in the doped nanocrystals. The desired lanthanum to terbium (La : Tb) molar ratio was 4 : 1 (80 : 20) since concentration quenching has been shown to occur when Tb^{3+} levels exceeded 20% of the total RE ion component of the inorganic host nanocrystal [37].

In order to maintain an 80/20 ratio of La : Tb so as to minimize the possibility of concentration quench, the calculated fluoride to lanthanum ratio was 4 : 1 and fluoride to terbium was 14 : 1. The importance of the fluoride content is related to its ability to act as a lattice stabilizer within the crystal allowing interspatial distance between the active ions [38]. All the experimental ratios were less than the calculated ratios. In the case of fluorine, this reduction could be attributed to the exchange of the fluoride anions with hydroxyl groups. The exchange between F and OH bonds throughout the nanoparticles is undesirable as a result of producing efficient deactivation pathways of the RE ion emissions [39].

4. Conclusions

PMMA nanocomposites were produced via solution/precipitation chemistry using ligand capped nanocrystals doped with Tb^{3+} ions. Two nanocomposite synthesis routes were evaluated with water being the solvent in Route 1 and methanol was used as the solvent in Route 2. The organic ligand (ASA and PA) and the inorganic nanocrystal (Tb^{3+}:LaF_3)

in the PMMA matrix were verified by ATR-FTIR spectroscopy and EDX analyses. PMMA nanocomposites produced with PA capped nanoparticles via synthesis Routes 1 and 2 exhibited absorption peaks that were not present in undoped PMMA. These peaks represented C–O stretching of the formed anion and the stretching vibrations of C–C bonds in the pyridine ring. For all the polymer nanocomposites loaded with ASA surface treated nanocrystals, C–H bond stretching of the aromatic ring structure produced absorption peaks that were not present in undoped PMMA. The EDX analysis confirmed the presence of Tb^{3+}, La^{3+}, and F in the doped nanocrystals of all of the polymer nanocomposites.

Conflict of Interests

The authors declare that there is no conflict of interests regarding the publication of the paper.

Acknowledgments

The authors acknowledge the support and funding provided by the National Science Foundation Award HRD-0450279, Center of Optical Materials Science and Engineering Technologies (COMSET), Department of Materials Science and Engineering at Clemson University, Center for Materials Science, and Department of Engineering at James Madison University. A note of gratitude is given to Courtney Kucera and Kim Ivey for their help with this work.

References

[1] L. H. Slooff, A. van Blaaderen, A. Polman et al., "Rare-earth doped polymers for planar optical amplifiers," *Journal of Applied Physics*, vol. 91, no. 7, pp. 3955–3980, 2002.

[2] H. Ma, A. K. Jen, and L. R. Dalton, "Polymer-based optical waveguides: materials, processing, and devices," *Advanced Materials*, vol. 14, pp. 1339–1365, 2002.

[3] J. Zubia and J. Arrue, "Plastic optical fibers: an introduction to their technological processes and applications," *Optical Fiber Technology*, vol. 7, no. 2, pp. 101–140, 2001.

[4] K. Peters, "Polymer optical fiber sensors—a review," *Smart Materials and Structures*, vol. 20, Article ID 013002, 2011.

[5] A. M. Glass, D. J. Digiovanni, T. A. Strasser et al., "Advances in fiber optics," *Bell Labs Technical Journal*, vol. 5, no. 1, pp. 168–187, 2000.

[6] L. G. Jacobsohn, C. J. Kucera, T. L. James et al., "Preparation and characterization of rare earth doped fluoride nanoparticles," *Materials*, vol. 3, no. 3, pp. 2053–2068, 2010.

[7] P. Wang, Y. Wang, and L. Tong, "Functionalized polymer nanofibers: a versatile platform for manipulating light at the nanoscale," *Light: Science and Applications*, vol. 2, article e102, 2013.

[8] H. Jiu, L. Zhang, G. Liu, and T. Fan, "Fluorescence enhancement of samarium complex co-doped with terbium complex in a poly(methyl methacrylate) matrix," *Journal of Luminescence*, vol. 129, no. 3, pp. 317–319, 2009.

[9] U. Resch-Genger, M. Grabolle, S. Cavaliere-Jaricot, R. Nitschke, and T. Nann, "Quantum dots versus organic dyes as fluorescent labels," *Nature Methods*, vol. 5, no. 9, pp. 763–775, 2008.

[10] J. Wang, S. Bo, L. Song, J. Hu, X. Liu, and Z. Zhen, "One-step synthesis of highly water-soluble LaF_3:Ln^{3+} nanocrystals in methanol without using any ligands," *Nanotechnology*, vol. 18, no. 46, Article ID 465606, 2007.

[11] D. Y. Kong, Z. L. Wang, C. K. Lin et al., "Biofunctionalization of CeF_3:Tb^{3+} nanoparticles," *Nanotechnology*, vol. 18, no. 7, Article ID 075601, 2007.

[12] M.-C. Daniel and D. Astruc, "Gold nanoparticles: assembly, supramolecular chemistry, quantum-size-related properties, and applications toward biology, catalysis, and nanotechnology," *Chemical Reviews*, vol. 104, no. 1, pp. 293–346, 2004.

[13] Y. Hiram and A. Nir, "A simulation of surface tension driven coalescence," *Journal of Colloid And Interface Science*, vol. 95, no. 2, pp. 462–470, 1983.

[14] F. C. J. M. Van Veggel, J. W. Stouwdam, G. A. Hebbink, and J. Huskens, "In Lanthanide(III)-doped nanoparticles that emit in the near infrared," in *Nanomaterials and Their Optical Applications*, vol. 5224 of *Proceedings of SPIE*, pp. 164–175, San Diego, Calif, USA, August 2003.

[15] F. S. Richardson, "Terbium(III) and europium(III) ions as luminescent probes and stains for biomolecular systems," *Chemical Reviews*, vol. 82, no. 5, pp. 541–552, 1982.

[16] Y. Luo, X. Yu, W. Su et al., "Energy transfer in a ternary system composed of $Tb(DBM)_3Phen$, $Eu(DBM)_3Phen$, and poly(N-vinylcarbazole)," *Journal of Materials Research*, vol. 24, no. 10, pp. 3023–3031, 2009.

[17] S. Maji and K. S. Viswanathan, "Ligand-sensitized fluorescence of Eu^{3+} using naphthalene carboxylic acids as ligands," *Journal of Luminescence*, vol. 128, no. 8, pp. 1255–1261, 2008.

[18] K. Gipson, C. Kucera, D. Stadther, K. Stevens, J. Ballato, and P. Brown, "The influence of synthesis parameters on particle size and photoluminescence characteristics of ligand capped Tb^{3+}:LaF_3," *Polymers*, vol. 3, no. 4, pp. 2039–2052, 2011.

[19] A. J. Kenyon, "Recent developments in rare-earth doped materials for optoelectronics," *Progress in Quantum Electronics*, vol. 26, no. 4-5, pp. 225–284, 2002.

[20] L. G. Jacobsohn, K. B. Sprinkle, C. J. Kucera et al., "Synthesis, luminescence and scintillation of rare earth doped lanthanum fluoride nanoparticles," *Optical Materials*, vol. 33, no. 2, pp. 136–140, 2010.

[21] B. Kokuoz, J. R. DiMaio, C. J. Kucera, D. D. Evanoff Jr., and J. Ballato, "Color kinetic nanoparticles," *Journal of the American Chemical Society*, vol. 130, no. 37, pp. 12222–12223, 2008.

[22] A. Alvarez-Ordóñez, D. J. M. Mouwen, M. López, and M. Prieto, "Fourier transform infrared spectroscopy as a tool to characterize molecular composition and stress response in foodborne pathogenic bacteria," *Journal of Microbiological Methods*, vol. 84, no. 3, pp. 369–378, 2011.

[23] H. Widiyandari, C. J. Hogan Jr., K. M. Yun, F. Iskandar, P. Biswas, and K. Okuyama, "Production of narrow-size-distribution polymer-pigment-nanoparticle composites via electrohydrodynamic atomization," *Macromolecular Materials and Engineering*, vol. 292, no. 4, pp. 495–502, 2007.

[24] H. G. Brittain, "Emission intensity of terbium(III) bound to benzene-carboxylic acid derivatives," *Journal of Luminescence*, vol. 17, no. 4, pp. 411–417, 1978.

[25] Y. Zhang, C. Gu, A. M. Schwartzberg, S. Chen, and J. Z. Zhang, "Optical trapping and light-induced agglomeration of gold nanoparticle aggregates," *Physical Review B: Condensed Matter and Materials Physics*, vol. 73, no. 16, Article ID 165405, 2006.

[26] J. Liu and Y. Li, "General synthesis of colloidal rare earth orthovanadate nanocrystals," *Journal of Materials Chemistry*, vol. 17, no. 18, pp. 1797–1803, 2007.

[27] J.-Y. Shim and V. K. Gupta, "Reversible aggregation of gold nanoparticles induced by pH dependent conformational transitions of a self-assembled polypeptide," *Journal of Colloid and Interface Science*, vol. 316, no. 2, pp. 977–983, 2007.

[28] I. G. Binev, B. A. Stamboliyska, and Y. I. Binev, "The infrared spectra and structure of acetylsalicylic acid (aspirin) and its oxyanion: an ab initio force field treatment," *Journal of Molecular Structure*, vol. 378, no. 3, pp. 189–197, 1996.

[29] M. Boczar, M. J. Wójcik, K. Szczeponek, D. Jamróz, A. Zięba, and B. Kawałek, "Theoretical modeling of infrared spectra of aspirin and its deuterated derivative," *Chemical Physics*, vol. 286, no. 1, pp. 63–79, 2003.

[30] R. Silverstein, G. Bassler, and T. Morrill, *Spectrometric Identification of Organic Compounds*, John Wiley & Sons, New York, NY, USA, 1991.

[31] J. A. Dean, in *Analytical Chemistry Handbook*, G. F. Nalven and V. L. Miller, Eds., McGraw-Hill, New York, NY, USA, 1995.

[32] V. V. Soman and D. S. Kelkar, "FTIR studies of doped PMMA—PVC blend system," *Macromolecular Symposia*, vol. 277, no. 1, pp. 152–161, 2009.

[33] G. Świderski, M. Kalinowska, S. Wojtulewski, and W. Lewandowski, "Experimental (FT-IR, FT-Raman, ^{1}H NMR) and theoretical study of magnesium, calcium, strontium, and barium picolinates," *Spectrochimica Acta Part A: Molecular and Biomolecular Spectroscopy*, vol. 64, no. 1, pp. 24–33, 2006.

[34] P. Koczoń, J. C. Dobrowolski, W. Lewandowski, and A. P. Mazurek, "Experimental and theoretical IR and Raman spectra of picolinic, nicotinic and isonicotinic acids," *Journal of Molecular Structure*, vol. 655, no. 1, pp. 89–95, 2003.

[35] J. Wang, S. Bo, L. Song, J. Hu, X. Liu, and Z. Zhen, "One-step synthesis of highly water-soluble LaF3:Ln^{3+} nanocrystals in methanol without using any ligands," *Nanotechnology*, vol. 18, no. 46, Article ID 465606, p. 6, 2007.

[36] J. D. Roberts and M. C. Caserio, "Separation and purification. Identification of organic compounds by spectroscopic techniques," in *Basic Principles of Organic Chemistry*, pp. 257–349, W. A. Benjamin, Menlo Park, Calif, USA, 1977.

[37] Z. L. Wang, Z. W. Quan, P. Y. Jia et al., "A facile synthesis and photoluminescent properties of redispersible CeF_3, CeF_3:Tb^{3+}, and CeF_3:Tb^{3+}/LaF_3 (core/shell) nanoparticles," *Chemistry of Materials*, vol. 18, no. 8, pp. 2030–2037, 2006.

[38] W. Viehmann, "Influence of charge compensation on uv excitation of rare-earth fluorescence," *The Journal of Chemical Physics*, vol. 47, no. 3, pp. 875–883, 1967.

[39] P. K. Sharma, R. Nass, and H. Schmidt, "Effect of solvent, host precursor, dopant concentration and crystallite size on the fluorescence properties of Eu(III) doped yttria," *Optical Materials*, vol. 10, no. 2, pp. 161–169, 1998.